Journal of Power Sources 196 (2011) 3623–3632

Contents lists available at ScienceDirect

Journal of Power Sources

journal homepage: www.elsevier.com/locate/jpowsour

Lithium bis(fluorosulfonyl)imide (LiFSI) as conducting salt for nonaqueous liquid electrolytes for lithium-ion batteries: Physicochemical and electrochemical properties

Hong-Bo Han[a], Si-Si Zhou[b], Dai-Jun Zhang[a,d], Shao-Wei Feng[a], Li-Fei Li[b], Kai Liu[a], Wen-Fang Feng[a], Jin Nie[a,*], Hong Li[b], Xue-Jie Huang[b,*], Michel Armand[c,**], Zhi-Bin Zhou[a,*]

[a] School of Chemistry and Chemical Engineering, Huazhong University of Science and Technology, 1037 Luoyu Road, Wuhan 430074, PR China
[b] Institute of Physics, Chinese Academy of Sciences, 3rd South Street, Zhongguancun, Beijing 100080, PR China
[c] Laboratoire de Réactivité et de Chimie des Solides (LRCS), CNRS 6007, UPJV, 33 rue St. Leu, 80039 Amiens, France
[d] Suzhou Fluolyte Co., Ltd, Yangtze River International Chemical Industrial Park, 7 Guangdong Road, 215634, Zhangjiagang, PR China

ARTICLE INFO

Article history:
Received 15 November 2010
Accepted 10 December 2010
Available online 21 December 2010

Keywords:
Lithium bis(fluorosulfonyl)imide
Nonaqueous electrolytes
Aluminum corrosion
Lithium-ion batteries

ABSTRACT

Lithium bis(fluorosulfonyl)imide (LiFSI) has been studied as conducting salt for lithium-ion batteries, in terms of the physicochemical and electrochemical properties of the neat LiFSI salt and its nonaqueous liquid electrolytes. Our pure LiFSI salt shows a melting point at 145 °C, and is thermally stable up to 200 °C. It exhibits far superior stability towards hydrolysis than $LiPF_6$. Among the various lithium salts studied at the concentration of 1.0 M (= mol dm^{-3}) in a mixture of ethylene carbonate (EC)/ethyl methyl carbonate (EMC) (3:7, v/v), LiFSI shows the highest conductivity in the order of LiFSI > $LiPF_6$ > $Li[N(SO_2CF_3)_2]$ (LiTFSI) > $LiClO_4$ > $LiBF_4$. The stability of Al in the high potential region (3.0–5.0 V vs. Li^+/Li) has been confirmed for high purity LiFSI-based electrolytes using cyclic voltammetry, SEM morphology, and chronoamperometry, whereas Al corrosion indeed occurs in the LiFSI-based electrolytes tainted with trace amounts of LiCl (50 ppm). With high purity, LiFSI outperforms $LiPF_6$ in both Li/$LiCoO_2$ and graphite/$LiCoO_2$ cells.

1. Introduction

Lithium hexafluorophosphate ($LiPF_6$) is used almost exclusively as conducting salt for state-of-the-art lithium-ion (Li-ion) batteries [1]. This is mainly attributed to the fact that the solutions of $LiPF_6$ in dipolar aprotic organic solvents, mainly including alicyclic carbonates (e.g., ethylene- and propylene-carbonate) and linear carbonates (e.g., dimethyl-, diethyl-, and ethyl-methyl-carbonate), or their mixtures, show high ionic conductivities, good electrochemical stability without aluminum (Al) current collector corrosion, though its thermal stability becomes problematic above 55 °C [1]. At relatively high temperatures, $LiPF_6$ is thermally instable and decomposes to produce pentafluorophosphorane (PF_5) through $LiPF_6$ (s) ⇒ LiF (s) + PF_5 (g) [3–5], which in turn reacts with solvents to generate highly toxic substances [2], or initiates polymerization of solvents [6–8]. Besides the thermal instability, $LiPF_6$ is extremely moisture sensitive [7–11]. In the carbonate-based dipolar aprotic solvents, the poorly solvated PF_6^- anion is highly reactive towards even weak nucleophiles; trace amounts of water (or alcohols) produce HF [7–11], which has detrimental effects on battery performances and safety. Therefore, new lithium salts with improved properties are highly desired to improve safety and lifetime, especially for large batteries in the automotive industry.

Over the past two decades, great efforts have been made to develop new lithium salts with improved chemical and/or electrochemical properties. Thus far, numerous weakly coordinating anions have been proposed as possible anion counterparts of lithium salts for Li-ion batteries, such as those containing nitrogen [12–14], phosphorus [15–20], carbon [21], or boron [22–32] as central atom, large cluster-based anions [33], and aromatic heterocyclics [34,35]. Among these candidates, three of them, lithium bis(trifluoromethanesulfonly) $Li[N(SO_2CF_3)_2]$ (LiTFSI) initially suggested by Armand and Kadiri [12] then commercialized by 3M® [13], lithium tris(pentafluoroethyl)-trifluorophosphate $Li[(C_2F_5)_3PF_3]$ (LiFAP) from Merck® [18,19], and lithium bis(oxalato)borate, $Li[B(C_2O_4)_2]$ (LiBOB) from Chemetall® [25], Xu and Angell [26–28], have been extensively studied in the hope of finding highly potential replacements for $LiPF_6$. Nevertheless, none of them as a single salt is superior to $LiPF_6$ when one

* Corresponding authors. Tel.: +86 27 87 55 94 27; fax: +86 27 87 54 36 32.
** Corresponding author.
E-mail addresses: niejin@mail.hust.edu.cn (J. Nie), xjhuang@aphy.iphy.ac.cn (X.-J. Huang), michel.armand@u-picardie.fr (M. Armand), zb-zhou@mail.hust.edu.cn (Z.-B. Zhou).

0378-7753/$ – see front matter © 2010 Elsevier B.V. All rights reserved.
doi:10.1016/j.jpowsour.2010.12.040

considers the overall performances for Li-ion batteries, because LiTFSI is corrosive towards Al current collector [13], LiBOB is not enough soluble in carbonate solvents [1,28], and the heavily fluorinated LiFAP may be too expensive and would lead to huge amounts of HF in case of battery fire.

Very recently, there has been a growing interest in lithium bis(fluorosulfonyl)imide Li[$N(SO_2F)_2$] (LiFSI) as conducting salt and its ionic liquids as non-flammable solvents for Li (or Li-ion) batteries [36–48], after the recognition that pure ionic liquid electrolytes based on the FSI^- anion, without any additives other than a lithium salt, are not only compatible with Li metal electrode [36] but also with graphitized carbon electrode for Li-ion batteries [37–39], which was not previously seen with ILs based on other anions. LiFSI was first claimed as conducting salt with good anticorrosive properties for Li-ion batteries in 1995 [49]; however, little attention was paid to it until recently [50,51], presumably due to the fact that it is rather difficult to prepare this salt with high purity in an unspecialized laboratory [52]. Very recently, various effective preparations for LiFSI and its derivatives have been reported by two groups [53–56], and considerable interest in this salt and its ionic liquids has been revived. While much work has been focused on understanding and designing its ionic liquids and gel electrolytes for Li (or Li-ion) batteries [36–47,51,52], little attention has been paid on studying the physicochemical and electrochemical properties of LiFSI itself, such as phase and thermal behavior, stability towards hydrolysis, and ionic transport behavior, which are fundamentally crucial for evaluating its applicability for electrolytes.

Since Al foil currently serves as a cathode current collector in today's commercial Li-ion batteries, it is a prerequisite that any salt of lithium for Li-ion batteries must be noncorrosive towards Al [13]. Although LiFSI has been appreciated as conducting salt for Li-ion batteries for long times [49], little work has been done on its corrosive property towards Al. Only very recently, it has been reported that LiFSI exhibited a corrosive potential as low as 3.3 V vs. Li^+/Li towards Al [48], which we suspected was caused by the presence of chloride (Cl^-) impurities in LiFSI arising from the preparative processes, but without further experimental confirmation.

In the present study, we wish to report on the study of the key physicochemical properties (phase transition, thermal stability, pyrolysis behavior, and stability towards hydrolysis) of the neat LiFSI salt, and the important physicochemical and electrochemical properties of its nonaqueous carbonate-based electrolytes (i.e., ionic conductivity and ion transport behavior, Al corrosion behavior, and performances of $Li/LiCoO_2$ and $graphite/LiCoO_2$ cells) for Li-ion batteries. In particular, the behavior of Al in the LiFSI-based electrolytes with high purity (Cl^- and HF < 1 ppm, H_2O < 30 ppm), and the impact of Cl^- impurities on Al corrosion in the LiFSI-based electrolytes were systematically investigated by cyclic voltammetry, SEM morphology, and chronoamperometry. Some of the properties of LiFSI were comparatively studied with those of the four typical salts, $LiPF_6$, LiTFSI, $LiClO_4$, and $LiBF_4$.

2. Experimental

2.1. General remarks

All the procedures related to the preparation of hygroscopic lithium salt, nonaqueous electrolyte solutions, electrochemical measurements, and cell assembly were carried out in an argon-filled glove box (Mikrouna, H_2O and O_2 < 1 ppm).

The following chemicals or materials were received as gratis, or purchased from various battery material makers: $LiPF_6$, $LiBF_4$, $LiClO_4$, CH_3CN, dimethylcarbonate (DMC), ethylene carbonate (EC), and ethyl methyl carbonate (EMC) (battery grade, H_2O < 20 ppm, Zhangjiagang Guotai-Huarong, China); lithium bis(trifluoromethane-sulfonyl)imide (LiTFSI, battery grade, Rhodia); bromothymol blue and tetra-*n*-butylammonium hydroxide in SeccoSolv® methanol (Alfa Aesar); anhydrous LiCl (99.9%, Alfa Aesar); Li foil and Li wire (China Energy Lithium Corp., Ltd.); standard graphite anode and $LiCoO_2$ cathode (Wuhan Lixun Power Corp., Ltd.); Al foil (99.99%, 0.5 mm thick, ATL, China); microporous polymeric separator (Celgard 2325). Toluene was distilled over Na prior to use.

Instrumental techniques used for characterizing LiFSI were as follows: ^{19}F (376.05 MHz) NMR spectra were recorded on a Bruker AV400 spectrometer, and acetone-d_6 was used as solvent. Chemical shift values are reported in ppm relative to external reference (CCl_3F). Element analyses (N and S) were performed on an Elementar Vario Micro Cube elemental analyzer. The content of impurities of F^- and Cl^- present in the prepared LiFSI salt was measured by ion chromatography (DIONEX ICS-1000, AS9-HC column). The level of HF remaining in the prepared LiFSI salt was estimated using a nonaqueous acid–base titration technique with bromothymol blue as indicator and tetra-*n*-butylammonium hydroxide in methanol as titrating reagent [18]. The water content in the prepared LiFSI salt was determined by Karl–Fischer titration (Metrohm KF 831).

The thermal behavior of LiFSI was measured on a combined system consisting of differential scanning calorimetry–thermogravimetry–mass spectrometry (DSC-TG-MS) (a NETSCH STA 449C instrument combined with NETSCH 403C Aeolos II quadrupole mass spectrometer). The samples were sealed in an Al crucible in a glove box, through which a pinhole was punched to allow gas escape for MS detection. Argon flow was purged for 1/2 h to remove the residual air in the test chamber before the DSC-TG-MS test. The test temperature increased from 30 to 500 °C at a rate of 10 °C min^{-1} under argon flow. Synchronically, the gaseous products formed during the pyrolysis were monitored by the on-line mass spectrometer. The temperature in the gas inlet system (transfer line and the furnace) was set at 300 °C. The system pressure was 2×10^{-5} mbar.

The phase behavior of nonaqueous electrolytes was measured on a NETZSCH 200F3 DSC instrument. The samples were hermetically sealed in an Al pan in a glove box, and then heated and cooled at a rate of 10 °C min^{-1} in the temperature range of −150 °C to 25 °C under nitrogen flow.

The viscosity (η) of nonaqueous electrolyte solutions was measured on a programmable viscometer (Brookfield, DV-III+) at 25 °C in a homemade dry chamber (H_2O < 10 ppm), and the temperature was accurately controlled to within ±0.1 °C using a Brookfield TC-502 oil bath.

The surface morphology of Al electrode was examined by SEM (Hitachi, S-570).

The size of anion counterpart of lithium salt used in the present work was approximately estimated from its van der Waals volume. Computation was performed using the HyperChem Professional 7 program package [57]. The geometry for each anion was fully optimized at the level of HF/6-31G (d). The van der Waals volume based on the optimized geometry was calculated, using the van der Waals radii of atoms adopted by Ue [58].

2.2. Preparation

Lithium bis(fluorosulfonyl)imide (LiFSI) was synthesized by a metathesis reaction between KFSI and $LiBF_4$ in DMC in nearly quantitative yield, similar to the preparation of its analogue, lithium (fluorosulfonyl)(pentafluoroethanesulfonyl)imide (LiFPFSI) [56]. Briefly, bis(fluorosulfonyl)imide ($HN(SO_2F)_2$) was obtained by fluorination of bis(chlorosulfonyl)imide ($HN(SO_2Cl)_2$) with SbF_3, which was converted to LiFSI by sequentially neutralization with K_2CO_3 in CH_3CN, and exchanged with $LiBF_4$ in DMC. The highly pure,

solvent-free LiFSI was obtained as white, flowing powder after recrystallization from DMC/toluene.

In an argon-filled glove box (H_2O and O_2 < 1 ppm), the electrolyte solutions were prepared by dissolving the requisite amount of lithium salt in a mixture of EC/EMC (3:7, v/v) in a PFA flask. The water content in the resulting electrolyte solutions was less than 30 ppm, determined by Karl–Fischer titration method.

2.3. Hydrolysis

The stability of LiFSI towards hydrolysis was comparatively studied with that of $LiPF_6$ under controlled conditions. Briefly, about 0.3% of water was added to the PFA flask containing 1.0 M LiFSI and $LiPF_6$ in a mixture of EC/EMC (3:7, v/v) at room temperature (Glassware must be excluded because of the corrosion nature of HF towards glass), and the PFA flask was well sealed and stored in a dry chamber (H_2O < 5 ppm) prior to test. The extent of hydrolysis was monitored by measuring the water content and HF level in the solutions at predetermined time intervals. The water content was determined by Karl Fischer titration, while the HF level was estimated using a nonaqueous acid–base titration technique, as described in literature [18]. Each of the reported values for the water content of HF level is the average of three measurements.

2.4. Electrochemical measurements

The ionic conductivities (σ) of electrolyte solutions were measured in a sealed platinum-black disk conductivity cell (cell constant: 9.96 cm^{-1}) using ac impedance technique. The ac impedance spectra were recorded on an Autolab PGSTAT302N impedance analyzer (Eco Chemie, Netherlands) in the frequency range from 10^{-2} to 10^6 Hz. The cell was calibrated with 0.1 M (= mol dm^{-3}) KCl aqueous solution. The temperature of the cell was accurately controlled to within ±0.1 °C using a JULABO F12 oil bath.

Cyclic voltammetry and chronoamperometry were performed on an Autolab PGSTAT302N electrochemical workstation (Eco Chemie, Netherland) using a three-electrode cell. Al foil (area = 0.30 cm^2) was used as working electrode, and Li metal served as both counter and reference electrodes in all the measurements. The cyclic voltammograms were measured between the open circuit potential (OCP) and 5.0 V vs. Li^+/Li at a scan rate of 1.0 mV s^{-1}, and the chronoamperometric profile was recorded at a constant polarization potential of 4.2 V vs. Li^+/Li.

2.5. Evaluation of Li and Li-ion cell

2032 coin-type stainless steel Li cells (Li/$LiCoO_2$) and Li-ion cells (graphite anode/$LiCoO_2$ cathode) were assembled using the corresponding electrodes, a microporous polymeric separator, and 1.0 M lithium salt in a mixture of EC/EMC (3:7, v/v) as electrolytes, respectively. The capacity of Li-ion cell was limited by the cathode, and its specific capacity was calculated according to the cathode materials. The performances of the cells were evaluated using a charge–discharge apparatus (Land, CT2001A) in a temperature-controlled dry room (25 ± 2 °C). All the cells were charged at a constant current (CC)–constant voltage (CV) mode, and discharged at a constant current (CC) mode between 2.75 and 4.2 V. All the cells were allowed to rest for 20 min in every charge/discharge cycle.

For rate capability test, the cells were subjected to three charge–discharge cycles at a rate of 0.2/0.2 C (1 C corresponding to 1.5 mA) for conditioning, and then discharged at 1 C, 1.5 C, and 2 C rates after being charged at a rate of 0.5 C. For cycling test, freshly prepared cells, after conditioning for three cycles at 0.2/0.2 C rate, were cycled at 0.5/0.2 C charge/discharge rate for 50 cycles.

Table 1
The characterization data of physicochemical properties for the neat lithium bis(fluorosulfonyl)imide (LiFSI) salt.

^{19}F NMR (ppm)	51.5
Appearance	White powder
Melting point (°C)[a]	135 (taken at onset), 145 (taken at peak)
Decomposition temperature (°C)[b]	200 (without mass loss), 312 (taken at 5% mass loss), 340 (taken at onset)
Elemental analysis (%)	Calculated (found): N, 7.49 (7.56); S, 34.28 (34.69)
Water content (ppm)	80
Impurities (ppm)	Cl^- (2.4); F^- (0.5); HF (0.1)

[a] Measured by DSC.
[b] Measured by TGA.

3. Results and discussion

3.1. Preparation and physicochemical properties of LiFSI

LiFSI was prepared in nearly quantitative yield by a metathesis reaction between high purity KFSI and $LiBF_4$ in DMC. The solvent-free LiFSI as white powder was obtained by recrystallisation from DMC upon addition of toluene, followed by vacuum drying at 50 °C.

The chemical structure and composition of the prepared LiFSI salt was confirmed by ^{19}F NMR, elemental analysis. The characterization data for the prepared LiFSI salt, and several kinds of trace amounts of impurities (F^-, Cl^-, HF, and H_2O) are summarized in Table 1. Especially, the content of impurities of F^-, Cl^- and HF occurring in the resulting LiFSI salt are lower than 0.5, 3, and 0.1 ppm, respectively, showing that the FSI^- anion is chemically stable and did not undergo decomposition or hydrolysis during the preparation processes. The superior stability of FSI^- anion was further demonstrated by hydrolysis test (see Section 3.2). As seen in Table 1, the purity of LiFSI prepared in this study is acceptable for electrolyte use.

The phase transition, thermal stability and pyrolysis behavior of the neat LiFSI salt was investigated by DSC-TG-MS under argon flow. The data for the melting point (T_m) and decomposition temperature (T_d) of LiFSI are presented in Table 1. Fig. 1 displays the DSC-TG-MS profiles of LiFSI. It shows a melting point at 145 °C as a sharp endothermic peak with an onset at 135 °C (Fig. 1a), both of which are obviously higher than the respective reported values of 132 [48] and 124–128 °C [54], indicating that LiFSI prepared in this study is of high purity. It is thermally stable up to 200 °C without mass loss on TGA (Fig. 1b) and detectable gaseous products on on-line MS (Fig. 1c). However, LiFSI starts to decompose above 200 °C, but shows only ≈3% mass loss from 200 to 300 °C, during which SO_2 (m/e = 64) is being detected as main gaseous products on on-line MS. The rate of decomposition becomes rapid from about 330 °C, as evidenced by the two consecutive exothermic peaks on the DSC trace. The radicals for SO_2 (m/e = 64) and NO_2 (m/e = 46) are instantaneously detected as main signals by on-line MS above 300 °C (Fig. 1c). The weight percentage of the residual is about 31%, which remains nearly constant to 520 °C, the end of pyrolysis test. It is unlikely to be a singly pure LiF solid, as the weight percentage of the residual (31%) on TGA obviously deviates from the stoichiometric ratio of LiF/LiFSI, and needs to be identified in future. All above results clearly indicate that the thermal stability of LiFSI is obviously higher than that for $LiPF_6$ (107 °C [5]) measured under similar conditions.

3.2. Hydrolysis

In order to test the stability of FSI^- anion towards hydrolysis in dipolar aprotic solvents, about 0.3% water was added to solutions of 1.0 M LiFSI in a mixture of EC/EMC (3:7, v/v) at room temperature. For comparison, a solution of 1.0 M $LiPF_6$ in a mixture of EC/EMC

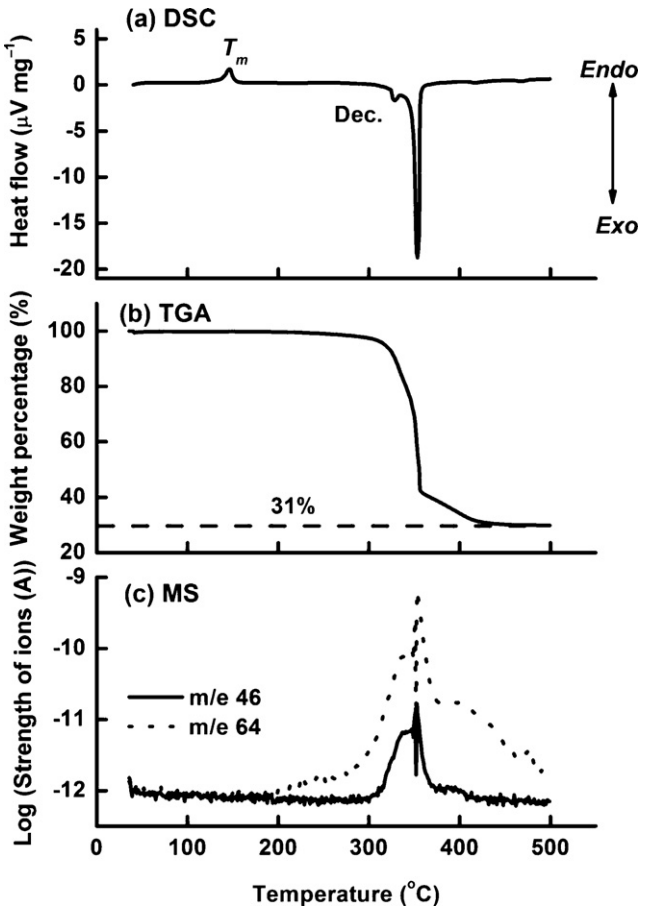

Fig. 1. DSC-TG-MS traces of the neat lithium bis(fluorosulfonyl)imide (LiFSI) salt.

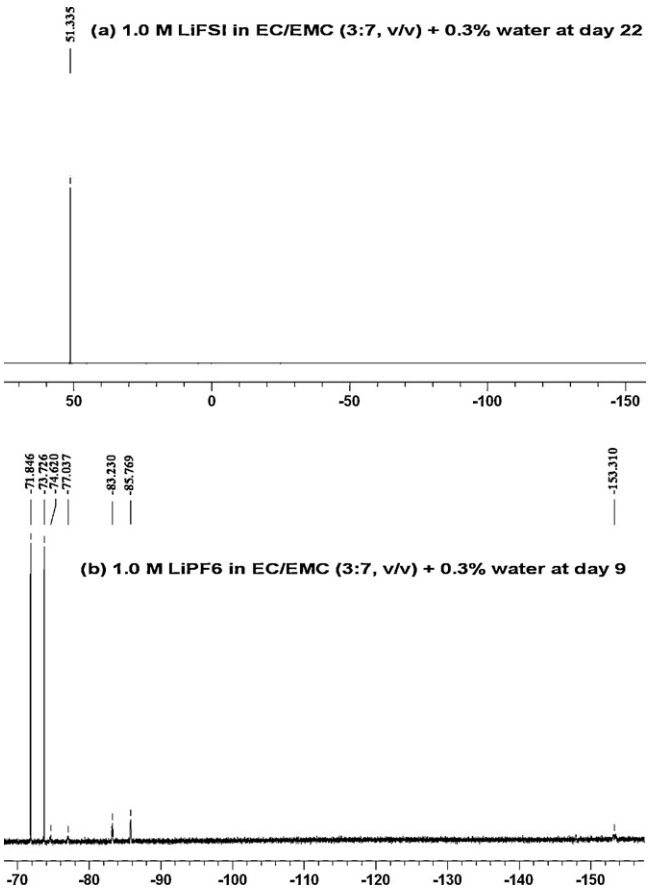

Fig. 3. ^{19}F NMR spectra of the electrolyte solutions after hydrolysis tests. (a) 1.0 M LiFSI in a mixture of EC/EMC (3:7, v/v) + 0.3% water at day 22. (b) 1.0 M $LiPF_6$ in a mixture of EC/EMC (3:7, v/v) + 0.3% water at day 9.

(3:7, v/v) was comparatively evaluated under the same conditions. Fig. 2 shows the time dependence of the water content and HF level in these two solutions, and Fig. 3 displays ^{19}F NMR spectra of these two solutions after the hydrolysis test. As seen in Fig. 2, both the water content and HF level in the LiFSI-based solutions remains almost constant over the whole period of evaluation (22 days). It is worthwhile noting that the HF level estimated from acid–base titration remains at an extremely low level (H^+ < 20 ppm) at the end of the hydrolysis test (at day 22), suggesting that the FSI^- anion does not hydrolyze during the hydrolysis test. Fig. 3a shows ^{19}F NMR spectrum of the LiFSI-based solutions at the end of the hydrolysis test (at day 22). There is only a single peak at the chemical shift value of δ_F = 51.3 ppm (i.e., F-SO_2- group of FSI^-) observed without any other signals. All these results clearly indicate that the FSI^- anion has a superior stability towards hydrolysis.

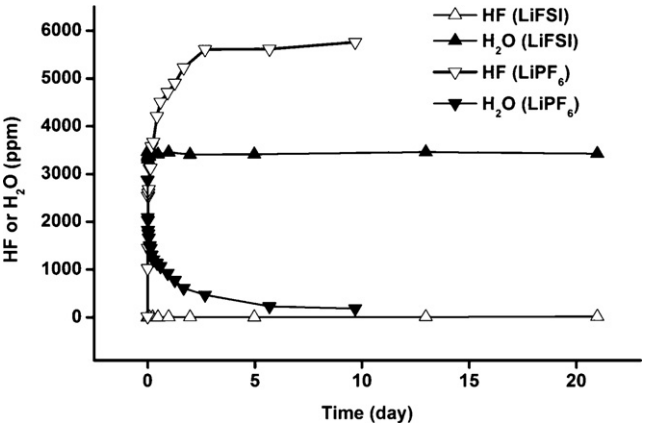

Fig. 2. Time dependence of the water content and HF level in the 1.0 M LiFSI and $LiPF_6$ in a mixture of EC/EMC (3:7, v/v) after addition of 0.3% water.

By contrast, in the $LiPF_6$-based solutions (Fig. 2), the water content decreases while the HF level increases rapidly in the first two days, and the added water has almost been completely consumed at day 9. This is essentially caused by the high reactivity of PF_6^- towards H_2O [10,11]. Fig. 3b displays ^{19}F NMR spectra of the $LiPF_6$-based solutions at the end of the hydrolysis test (day 9). As seen in Fig. 3b, while the typical doublet for PF_6^- at the chemical shift value of δ_F = 72.8 ppm (J_{F-P} = 707 Hz) is observed, the signals for its hydrolysis products are also detected (i.e., at the respective chemical shift values of δ_F = 75.8 ppm (doublet, J_{F-P} = 908 Hz) for PO_3F^{2-}, δ_F = 84.4 ppm (doublet, J_{F-P} = 955 Hz) for $PO_2FO_2^-$, and δ_F = 153.2 ppm (broad) for HF). The characterization data for the hydrolysis products of PF_6^- are consistent with the reported results for $LiPF_6$ in propylene carbonate (PC)-DMC-H_2O system [11].

3.3. Physicochemical properties of nonaqueous electrolyte solutions

For better understanding ionic conduction and transport behavior of LiFSI in nonaqueous electrolytes, its electrolyte solutions were comparatively studied with those of the four typical salts, $LiPF_6$, LiTFSI, $LiClO_4$, and $LiBF_4$, at the concentration of 1.0 M in a mixture of EC/EMC (3:7, v/v), in terms of their specific conductivities, viscosities, and glass transitions. The data of specific conductivities and viscosities at 25 °C, and glass transition temperatures (T_g)

Table 2
Viscosity, ionic conductivity, glass transition temperatures, van der Waals volume of anions, and the parameters for VTF function of 1.0 M lithium salt in EC/EMC (3:7, v/v).

Salt	η^a (cP)	σ^b (mS cm^{-1})	$V_a{}^c$ (Å^3)	$T_g{}^d$ (K)	$\sigma(T) = \frac{A}{\sqrt{T}} e^{-B/(T-T_0)}$		
					T_0 (K)	A (S m^{-1} K$^{1/2}$)	B (K)
LiFSI	2.96	9.73	95	170	145	2.69	423
$LiPF_6$	3.00	9.33	69	193	153	2.86	418
LiTFSI	3.40	7.57	147	156	151	2.10	408
$LiClO_4$	2.77	6.26	55	152	137	2.54	509
$LiBF_4$	2.23	3.72	49	154	127	1.55	543

[a] Viscosity at 25 °C.
[b] Ionic conductivity at 25 °C.
[c] van der Waals volume of anions estimated using the Hyperchem software.
[d] Glass transition temperature by DSC.

measured by DSC for all these electrolyte solutions are presented in Table 2. In addition, to see a possible correlation between the anion sizes of lithium salts and ionic conductivities, the values for the anion sizes are also included in Table 2, which were approximately estimated from their van der Waals volumes using the Hyperchem® software (see Section 2). It has been illustrated by Ue et al. [58] that the van der Waals volume is an acceptable measure to estimate ion size.

Fig. 4 compares Arrhenius plots of the electrolytes containing various lithium salts (1.0 M) in a mixture of EC/EMC (3:7, v/v) in the temperature range of −20 to 60 °C. The specific conductivities generally decrease in the order of LiFSI > $LiPF_6$ > LiTFSI > $LiClO_4$ > $LiBF_4$ in the measured temperature range. This trend in conductivity would be a combinational result of several competing factors that affect the conductivity including the degree of ionic association, viscosity, and anion size. A high degree of salt dissociation is favorable for enhancing the concentration of mobile ions, thus improving conductivity, whereas a high viscosity, and/or large anion size would impede ion transport, thus causing low conductivity. Among these five salts studied, LiFSI shows the highest conductivity, which is essentially attributed to its higher dissociation, a relatively low viscosity of its solutions, and a medium-range size for FSI^- (Table 2). $LiPF_6$ shows a little lower conductivity than LiFSI, though the size of $PF_6{}^-$ (69 Å^3) is smaller than that of FSI^- (95 Å^3), and the viscosity of electrolytes for $LiPF_6$ is comparable with that for LiFSI (i.e., 3.00 cP ($LiPF_6$) vs. 2.96 cP (LiFSI) at 25 °C) (Table 2). This may be explained by a higher degree of ionic association (or ion-pairing) for $LiPF_6$, which predominates over the anion size and viscosity in determining the conductivity. The impact of degree of ionic association on the conductivity is more significant for the two remaining salts, $LiClO_4$ and $LiBF_4$, both of which are much less conductive (Table 2 and Fig. 4). Although the solutions of both $LiClO_4$ and $LiBF_4$ have the lowest viscosities and smallest anion sizes (Table 2), they have the lowest transport kinetics of the series. It seems that a higher degree of ionic association for the latter plays a predominant role in determining the conductivity [59]. LiTFSI shows a lower conductivity than $LiPF_6$ (Table 2 and Fig. 4), though the association constant for LiTFSI is lower than that for $LiPF_6$ [59]. This would be the consequence of higher viscosities for the LiTFSI-based solutions and a larger anion size (see Table 2) for the $TFSI^-$ anion, which prevails over its better dissociation. From all above results, we could conclude that (1) among all the lithium salts reported in literature, LiFSI is one of the most dissociated salts in organic carbonate solvents, as indicated by its highest conductivities in the present study, and would also be a good model to guide designing new salts with high conductivity in future; and (2) in search of highly conductive lithium salts used for Li-ion batteries, more attention should be paid to the weakly coordinating anion with a medium-range size, while large anions, despite their weakly coordinating nature, would cause a highly viscous electrolyte solutions, thus low conductivity like $[(C_2F_5)_3PF_3]^-$ (FAP^-) [18].

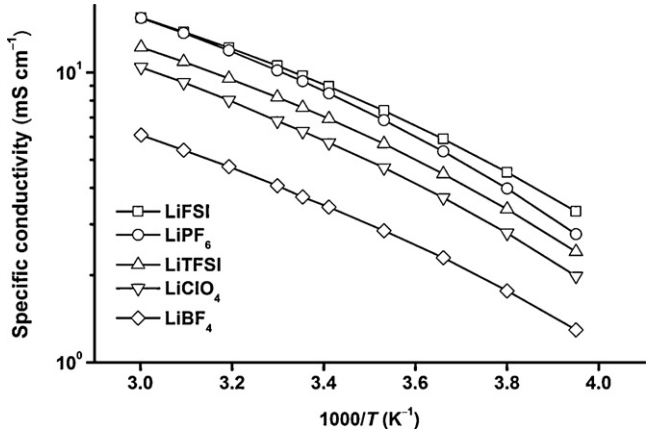

Fig. 4. Arrhenius plots of specific conductivity of 1.0 M LiFSI, $LiPF_6$, LiTFSI, $LiClO_4$, and $LiBF_4$ in a mixture of EC/EMC (3:7, v/v).

As seen in Fig. 4, the temperature dependence of specific conductivities in Arrhenius coordinates for all the electrolytes displays a nonlinear profile in the measured temperature range of −20 to 60 °C, which is also observed in nonaqueous electrolytes in high concentration regions [60–62]. Therefore, we correlate the specific conductivities of these electrolyte solutions with the empirical Vogel–Tammann–Fulcher (VTF) equation [63], Eq. (1):

$$\sigma(T) = \frac{A}{\sqrt{T}} e^{-B/(T-T_0)} \quad (1)$$

wherein A and B are constants, of which the former is a pre-exponential factor proportional to $T^{-1/2}$, and B is related to the critical free volume for ion transport. T_0 is the ideal glass transition temperature, at which the configurational entropy of the liquid vanishes [64] or the temperature at which the free volume of the liquid disappears [65] and all fluid properties cease to exist, implying that the function is nonlinear as T approaches T_0. Fig. 5 shows VTF plots of the electrolytes in Table 2, which was obtained by best fitting the experimental values to Eq. (1). Indeed, excellently linear relationships (correlation coefficient $r^2 > 99.99\%$) are obtained between the two parameters, $\ln(\sigma T^{1/2})$ and $1/(T - T_0)$, for all the electrolytes (see Fig. 5), and the values for all the parameters in Eq. (1) are summarized in Table 2. These results suggest that ion transport in these nonaqueous liquid electrolytes is highly correlated with the motion of solvent molecules, and obeys a free-volume, solvent-assisted ionic conduction mechanism [60,61], because of the strong interactions between Li^+ cations and solvent molecules, as explained in previous reports [60,61].

Fig. 6 shows the DSC traces of the electrolytes containing various salts in Table 2. All the electrolyte solutions are glass-forming liquids, and their glass transition temperatures (T_g) measured by DSC are presented in Table 2. As seen in Table 2, the values of T_g

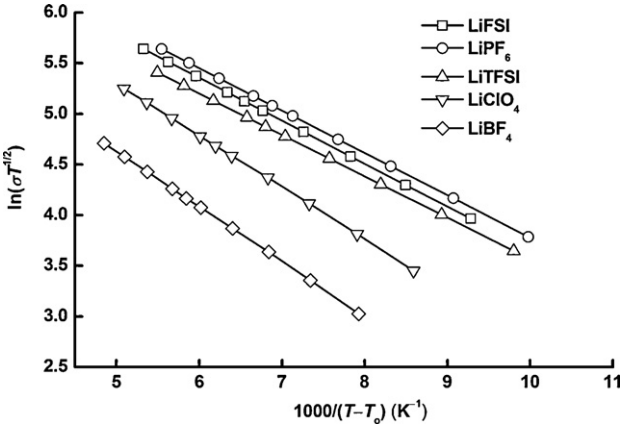

Fig. 5. VTF plots of specific conductivity for 1.0 M LiFSI, $LiPF_6$, LiTFSI, $LiClO_4$, and $LiBF_4$ in a mixture of EC/EMC (3:7, v/v). The values used in these plots are extracted from best fitting of the conductivity-temperature data.

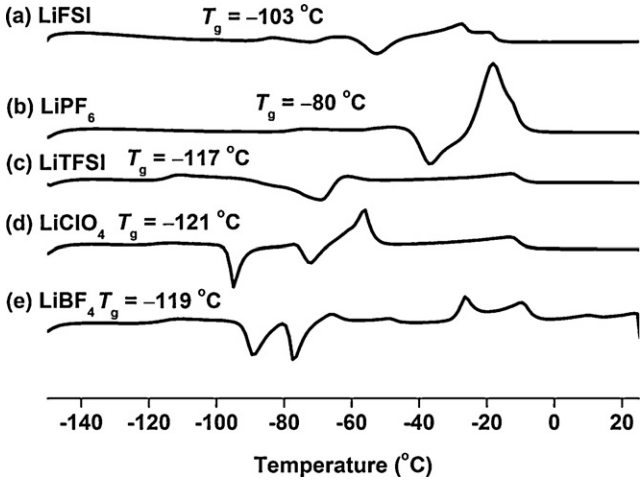

Fig. 6. DSC traces on heating for electrolyte solutions of 1.0 M lithium salt in a mixture of EC/EMC (3:7, v/v). (a) LiFSI, (b) $LiPF_6$, (c) LiTFSI, (d) $LiClO_4$, (e) $LiBF_4$.

obtained from the DSC measurements are all higher by a magnitude of 20–50 °C than those of the corresponding T_0 derived from Eq. (1), except for that for LiTFSI. This is consistent with the reported results, where the values of T_0 are usually $0.7–0.9 \times T_g$ [66]. It is noteworthy that both the T_0 and T_g values are lower for LiFSI than for $LiPF_6$, thus the drop in conductivity for LiFSI at low temperatures would be minimized, portending good rate capabilities for Li-ion batteries in low temperature region. Fig. 4 effectively shows that the LiFSI curve for conductivity separates markedly above that of $LiPF_6$ at −20 °C.

3.4. Anodic behavior of Al in nonaqueous electrolyte solutions

In order to investigate Al behavior in the LiFSI-based electrolytes reliably, the corrosion behavior of Al was first studied in the LiFSI-based electrolytes with high purity (Cl^- and HF < 1 ppm, H_2O < 30 ppm), in which the possible effect on Al corrosion arising from the impurities of Cl^-, H^+ and H_2O could be negligible. Then, the impact of Cl^- on Al corrosion was investigated by addition of trace amounts of anhydrous LiCl (50 ppm) into the highly pure

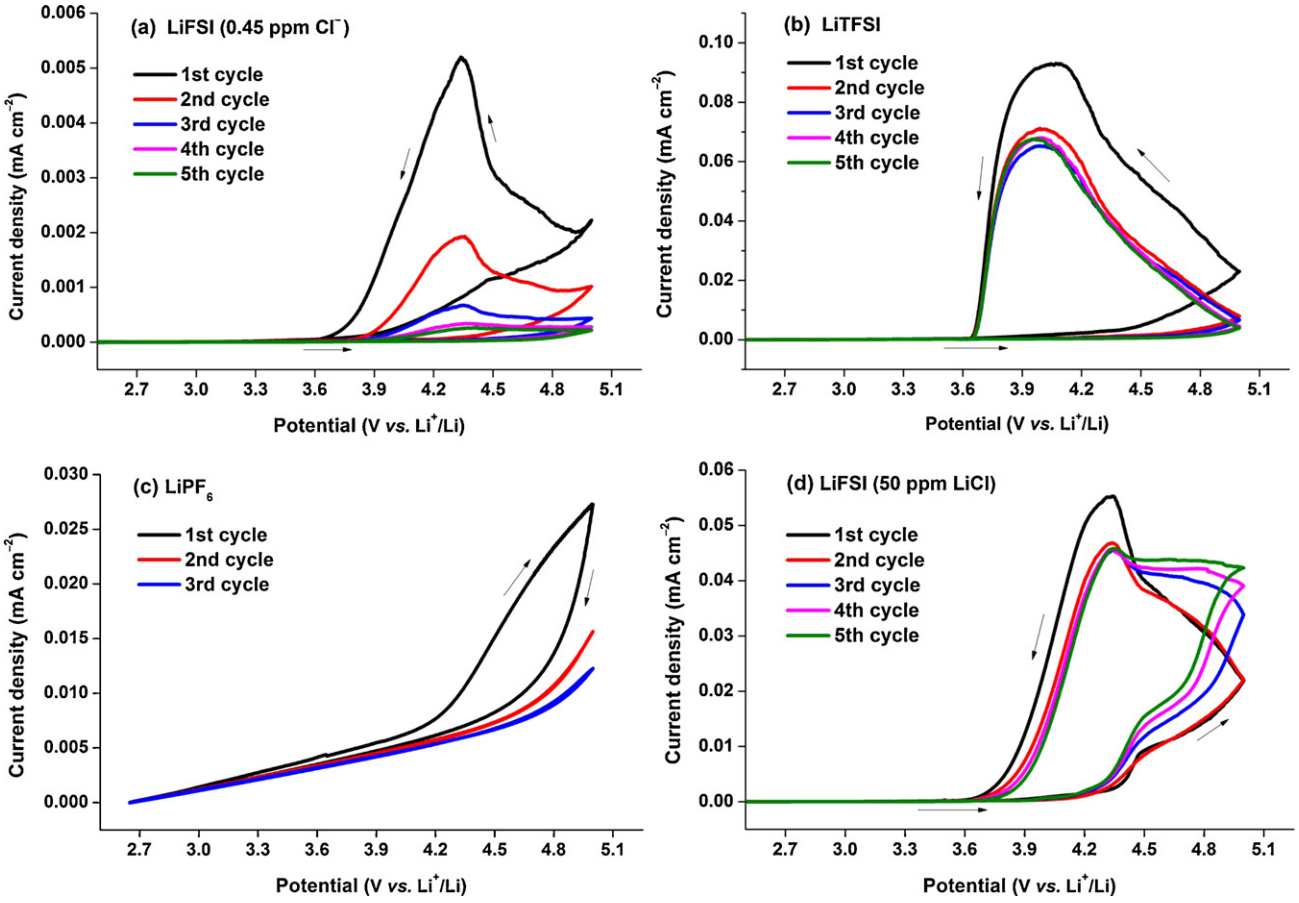

Fig. 7. Cyclic voltammograms for Al foil in electrolytes of 1.0 M lithium salt in a mixture of EC/EMC (3:7, v/v). Scan rate: 1.0 mV s^{-1}; (a) LiFSI (0.45 ppm Cl^-), (b) LiTFSI, (c) $LiPF_6$ and (d) LiFSI (50 ppm LiCl).

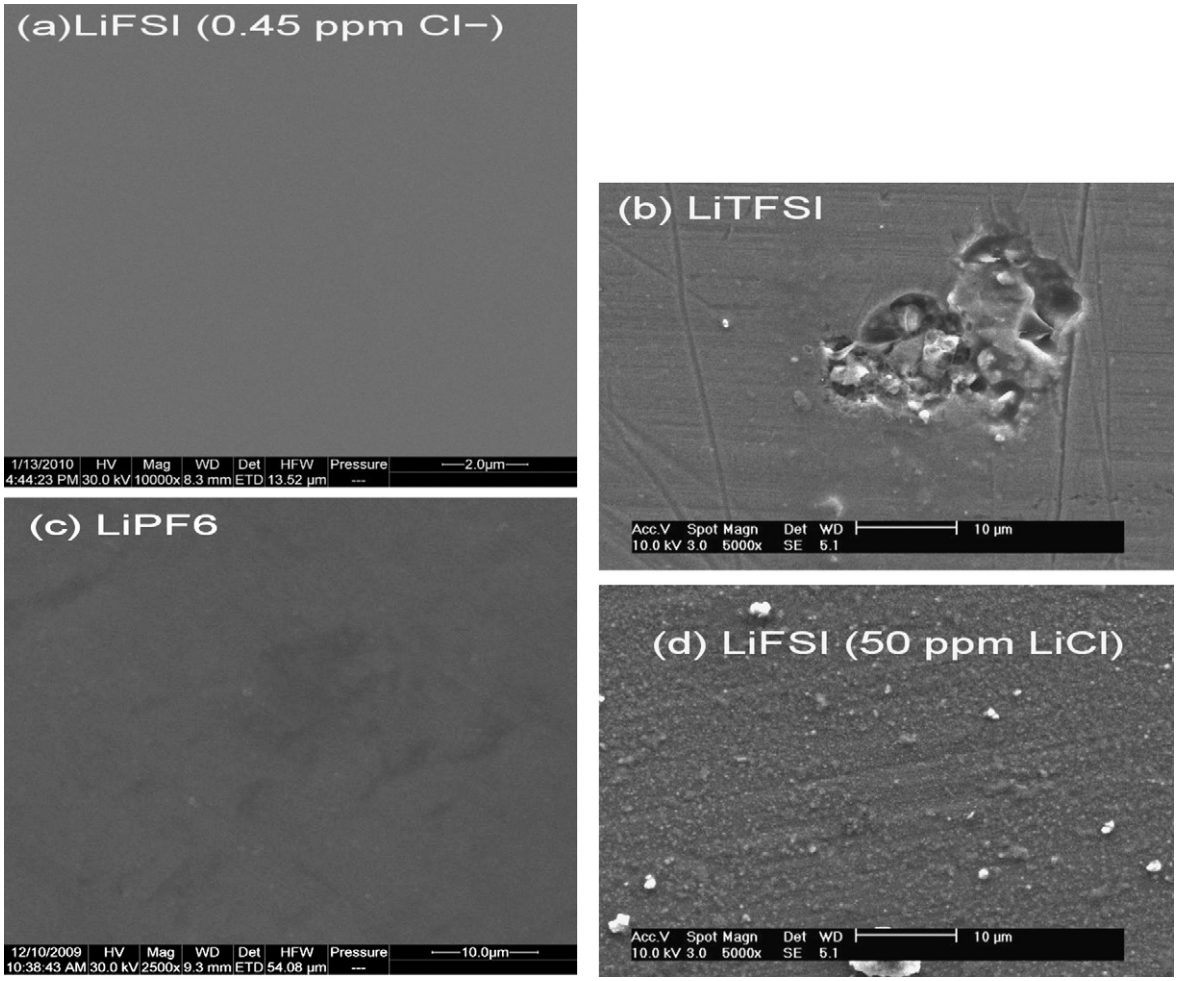

Fig. 8. SEM images of Al electrode after the potential cycling in electrolytes of 1.0 M lithium salt in a mixture of EC/EMC (3:7, v/v). Before the measurement, the sample was well rinsed by DMC in the glove box, and then dried at room temperature under vacuum for 12 h. (a) LiFSI (0.45 ppm Cl^-), (b) LiTFSI, (c) $LiPF_6$ and (d) LiFSI + 50 ppm LiCl.

LiFSI-based electrolytes. For comparison, the corrosion behaviors of Al in the corresponding LiTFSI- and $LiPF_6$-based solutions were also examined under the same experimental conditions.

Fig. 7 compares the cyclic voltammograms of Al electrode in 1.0 M LiFSI, $LiPF_6$, LiTFSI, and LiFSI containing 50 ppm LiCl in a mixture of EC/EMC (3:7, v/v), in the first few consecutive scans. In the LiFSI-based solutions with high purity (Fig. 7a), the responses of current to potential scan (*I*–*V*) show a hysteresis loop initiated at about 3.7 V vs. Li^+/Li, with a small peak current (0.0052 mA cm^{-2}) at about 4.35 V at the reverse cathodic scan of the first cycle. With further cycling, the initiation potentials of the hysteresis loop move significantly to more anodic side, while the peak currents sharply decrease. In particular, no significant anodic current is detected up to 4.5 V at the 5th cycle (Fig. 7a). These results strongly suggest that no severe corrosion occurred on the surface of Al, and Al passivation would be achieved in the LiFSI-based electrolytes with high purity.

Quite different behavior is seen in Fig. 7b for Al in the LiTFSI-based solutions, in comparison with that in Fig. 7a for LiFSI. A large hysteresis loop (note vertical scale differences between Fig. 7a and b) initiated around 3.7 V vs. Li^+/Li is observed for every cycle, which is indicative of Al corrosion [13,67,68]. The initiation potential (3.7 V vs. Li^+/Li) of the hysteresis in Fig. 7b is consistent with the values reported in literature [13,67–69]. As seen in Fig. 7b, the huge anodic currents, which are larger by 1–2 orders of magnitude than those observed in the LiFSI-based solutions (see Fig. 7a and b), do not decrease with cycling. Similar phenomena for LiTFSI were also observed in previous study [68]. This clearly indicates that Al corrosion indeed occurred in the high potential region, and became more and more serious with cycling in the LiTFSI-based electrolytes.

Fig. 7c shows the cyclic voltammograms of Al in the $LiPF_6$-based electrolytes. The anodic current is a little higher than that obtained in the LiFSI-based solutions (see Figs. 7a and c). Notably, the currents are lower for the reverse cathodic scan than those for the upward anodic scan (in contrast to Figs. 7a and b), and become smaller in the subsequent cycles. This is the typical characteristic of forming passive layer on the surface of Al, which conforms to the results in previous reports [67,70].

Fig. 7d displays the cyclic voltammograms of Al in the electrolytes of 1.0 M LiFSI in a mixture of EC/EMC (3:7, v/v) after addition of 50 ppm LiCl. The significant impact of Cl^- on Al corrosion is immediately manifested, when we compare the current responses in Fig. 7d with those in Fig. 7a. Upon addition of 50 ppm LiCl into the LiFSI-based electrolytes, much larger hysteresis loops initiated around 3.7 V vs. Li^+/Li, accompanying large anodic currents, are observed for each cycle. These phenomena are quite similar to those observed in Fig. 7b for the corrosive LiTFSI salt [68], and also concur with the results reported in literature [48], where the Cl^- impurities were suspected to have occurred in the prepared LiFSI salt. All these experimental evidences clearly indicate that serious Al corrosion did occur, due to the occurrence of trace amounts of Cl^- in the LiFSI-based electrolytes. It is worthwhile noting that the protective potential of Al for LiFSI (i.e., the initiated point of the hysteresis loop in cyclic voltammogram in Figs. 7a and d) obtained in this study is 3.7 V vs. Li^+/Li, which is

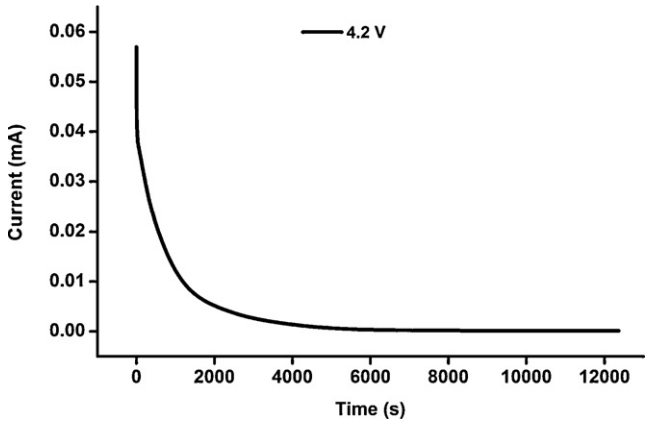

Fig. 9. Chronoamperometry profile of Al foil electrode obtained at 4.2 V vs. Li^+/Li in electrolytes of 1.0 M LiFSI in a mixture of EC/EMC (3:7, v/v).

obviously higher than that 3.3 V vs. Li^+/Li reported in recent literature [48]. This discrepancy would be partially attributed to some other unknown impurities, beside the Cl^- ions, present in the LiFSI salt used in previous report [48], an hypothesis which is supported by the lower value of melting point (132 °C [48] vs.145 °C in this study, both taken at the peak of DSC trace) reported in previous work. Therefore, when one considers LiFSI to be used for Li-ion batteries, trace amounts of deleterious impurities towards Al, such as Cl^- and H_2O, must be strictly excluded from it.

Fig. 8 displays the SEM images of the corresponding Al foil after above cyclic voltammetry tests (see Fig. 7). As can be seen in Fig. 8, the surfaces of Al in both the LiFSI- and $LiPF_6$-based electrolytes are very smooth without any corrosion after several cycles, whereas serious corrosion on the surface of Al has been observed for the electrolytes of LiTFSI and LiFSI containing 50 ppm LiCl, as indicated by the large pitting-corrosion holes (Fig. 7c) and roughness (Fig. 7d) occurring on the surface of Al.

To further approve the good compatibility of Al with LiFSI, potentiostatic experiment was conducted on Al electrode in the LiFSI-based electrolytes. Fig. 9 shows the chronoamperometric profile recorded at the constant polarization potential of 4.2 V vs. Li^+/Li. The anodic currents decrease sharply at the first 2000 s, and gradually decrease further in the subsequent 6000 s, and finally remain almost constant at an extremely low level of current. The chronoamperometric responses for LiFSI are quite similar to those observed for the reported noncorrosive imide salts, such as $Li[N(SO_2C_2F_5)_2]$ (LiBETI) and $Li[N(SO_2CF_3)(SO_2C_4F_9)]$ [13]. This indicates that both Al and the LiFSI-based electrolytes are stable at the potential of 4.2 V vs. Li^+/Li, which is pivotal for LiFSI used as conducting salt for 4 V class Li-ion batteries. All the above results obtained from the experiments of cyclic voltammetry, SEM morphology, and chronoamperometry suggest that 1) LiFSI is not an "aggressive" salt towards Al, and the passivation of Al could be achieved in the LiFSI-based electrolyte solutions, and 2) trace amounts of Cl^-, even at the level of 50 ppm, in the LiFSI-based electrolytes, would cause serious Al corrosion.

3.5. LiFSI as electrolyte salt for Li and Li-ion cells

As the LiFSI salt prepared in this study is of high purity and does not corrode Al, as demonstrated above (see Section 3.4), it is further used for battery test. The performances of LiFSI as conducting salt for Li and Li-ion batteries were evaluated, and were comparatively studied with those of the corresponding $LiPF_6$, using 2032 coin-type Li/$LiCoO_2$ half-cells and graphite/$LiCoO_2$ full Li-ion cells, at room temperature.

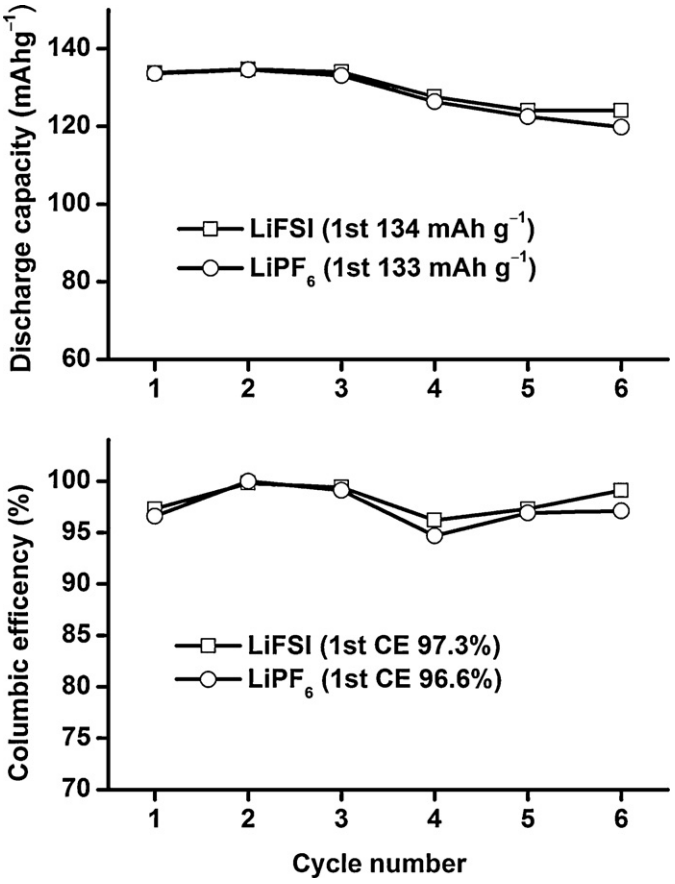

Fig. 10. Discharge capacities and columbic efficiencies of Li/$LiCoO_2$ half-cell vs. cycle number using 1.0 M LiFSI and $LiPF_6$ in a mixture of EC/EMC (3:7, v/v). Charge rate: 0.2 C (1st–3rd cycle), 0.5 C (4–6th); discharge rate: 0.2 C (1st–3rd cycle), 1 C (4th), 1.5 C (5th), 2 C (6th).

Fig. 10 shows the discharge capacities and columbic efficiencies (CEs) of Li/$LiCoO_2$ half-cells using LiFSI and $LiPF_6$ in the first few cycles at different discharge rates. The corresponding charge/discharge profiles for the LiFSI-based cell are presented in Fig. 11. The columbic efficiency for the LiFSI-based cell at the first cycle is 97.3%, which is slightly higher than that 96.6% for the $LiPF_6$-based one, and both of the cells nearly reach 100% efficiency at the second cycle, suggesting that stable electrolyte/electrode interface has been achieved in both the LiFSI- and $LiPF_6$-based electrolytes.

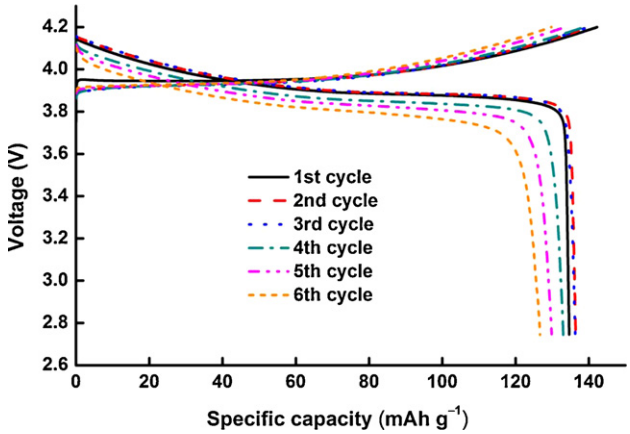

Fig. 11. Charge/discharge profiles of Li/$LiCoO_2$ half-cell using 1.0 M LiFSI in a mixture of EC/EMC (3:7, v/v). Charge rate: 0.5 C; discharge rate: 0.2 C (1st–3rd cycle), 1 C (4th), 1.5 C (5th), 2 C (6th).

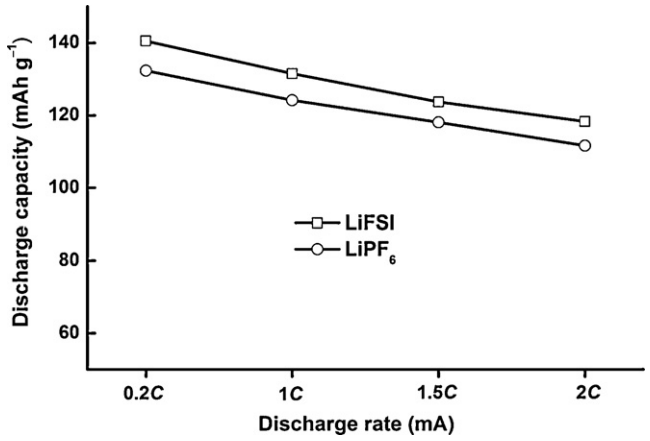

Fig. 12. Discharge capacities of graphite/$LiCoO_2$ Li-ion cells using 1.0 M LiFSI and $LiPF_6$ in a mixture of EC/EMC (3:7, v/v) at different discharge rates after being charged at 0.5 C.

As seen in Fig. 10, the discharge capacities for both the LiFSI- and $LiPF_6$-based cells are comparable, close to the theoretical capacity (138 mAh g^{-1}) in the first three cycles. The capacities fade with the increase of discharge current (the 4th–6th cycles), and the LiFSI-based cell shows a slightly better rate capability than the $LiPF_6$-based one at the rates above 1.5 C, likely due to the better conductivities for the LiFSI-based electrolytes. This is consistent with the results of the Li/$LiFePO_4$ cells using 1 M LiFSI and $LiPF_6$ in EC/diethyl carbonate (DEC) [39].

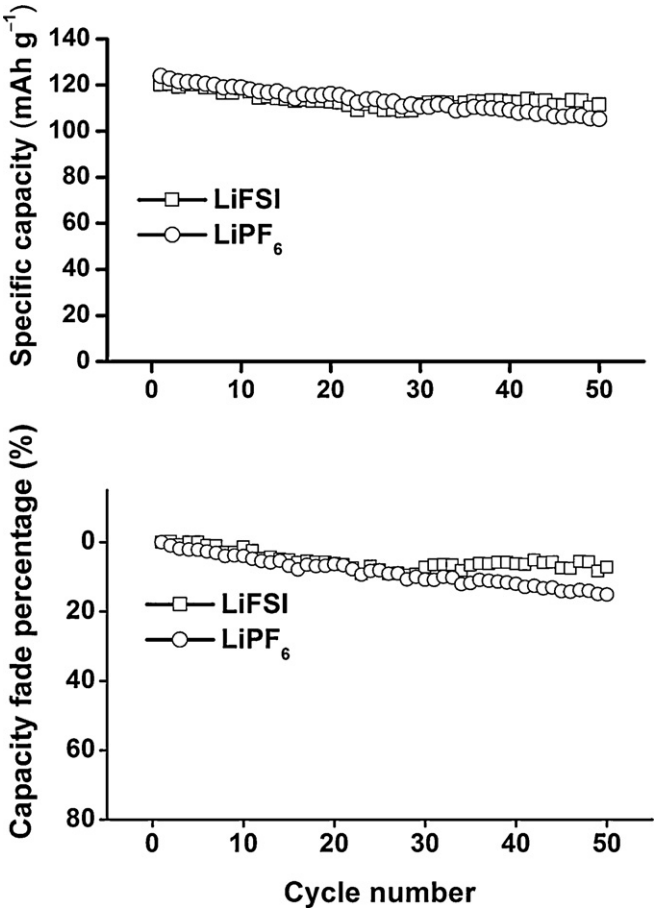

Fig. 13. Specific capacity and capacity fade vs. cycle number for graphite/$LiCoO_2$ Li-ion cells using 1.0 M LiFSI and $LiPF_6$ in a mixture of EC/EMC (3:7, v/v). Charge/discharge rate 0.5/0.2 C.

Fig. 12 shows the discharge capacities of the graphite/$LiCoO_2$ Li-ion cells using LiFSI and $LiPF_6$, respectively, at various discharge rates, after conditioning. At all discharge rates, the discharge capacities of the LiFSI-based cell are all higher than those of the $LiPF_6$-based one, which could be attributed to the higher conductivities of the LiFSI-based electrolytes, and lower resistance of the SEI layer formed in the LiFSI-based electrolytes [39].

Fig. 13 compares the cycling performances (capacity vs. cycle number) of the cells using LiFSI and $LiPF_6$, respectively. Although both of the cells exhibit an almost equivalent capacity at the first cycle, the LiFSI-based cell sustains more stable discharge capacities than the $LiPF_6$-based one upon cycling. The total capacity-fading rate at the 50th cycle for the LiFSI-based cell is 7%, while that for the $LiPF_6$-based one is 15%. These results indicate that LiFSI can afford a better cycling performance than $LiPF_6$ for 4 V class Li-ion cells, which would be attributable to more stable properties for LiFSI, including higher thermal stability and less sensitivity to moisture (see Table 1 and Figs. 1–3).

4. Conclusions

Lithium bis(fluorosulfonyl)imide Li[$N(SO_2F)_2$] (LiFSI) with high purity has been prepared and characterized. The neat LiFSI salt shows a melting point at 145 °C, and is thermally stable up to 200 °C without mass loss. LiFSI shows much better stability towards hydrolysis and higher conductivities than $LiPF_6$ in organic carbonate solvents, due to its better chemical stability and higher dissociation, and a medium-range anion size for FSI^-. The liquid carbonate electrolytes made from LiFSI do not corrode Al in the high potential region of 3–5 V vs. Li^+/Li, and the passivation of Al can be achieved at 4.2 V vs. Li^+/Li; however, Al corrosion can be induced when trace amounts of LiCl (50 ppm) are added into the electrolytes. Under the same conditions, the performances of both the Li/$LiCoO_2$ and graphite/$LiCoO_2$ cells are better for LiFSI than for $LiPF_6$. As both the T_0 of the VTF law and T_g values are lower for LiFSI than for $LiPF_6$, the drop in conductivity at low temperatures would be minimized, thus portending good rate capabilities below −20 °C. All these promising performances suggest that LiFSI is a highly promising electrolyte salt for Li-ion batteries.

Acknowledgements

This work was supported by the National Natural Science Foundation of China (No. 50873041), the National High Technology Research and Development Program of China (No. 2007AA03Z246), and the State Key Laboratory of Materials Processing, Die and Mould Technology, Huazhong University of Science and Technology.

References

[1] K. Xu, Chem. Rev. 104 (2004) 4303.
[2] A. Hammami, N. Raymond, M. Armand, Nature 424 (2003) 635.
[3] C.G. Barlow, Electrochem. Solid-State Lett. 2 (1999) 362.
[4] E. Zinigrad, L. Larush-Asraf, J.S. Gnanaraj, M. Sprecher, D. Aurbach, Thermochim. Acta 438 (2005) 184.
[5] H. Yang, G.V. Zhuang, P.N. Ross Jr., J. Power Sources 161 (2006) 573.
[6] S.E. Sloop, J.K. Pugh, S. Wang, J.B. Kerr, K. Kinoshita, Electrochem. Solid-State Lett. 4 (2001) A42.
[7] C.L. Campion, W. Li, B.L. Lucht, J. Electrochem. Soc. 152 (2005) A2327.
[8] J.S. Gnanaraj, E. Zinigrad, L. Asraf, H.E. Gottlieb, M. Sprecher, M. Schmidt, W. Geissler, D. Aurbach, J. Electrochem. Soc. 150 (2003) A1533.
[9] U. Heider, R. Oesten, M. Jungnitz, J. Power Sources 81 (1999) 119.
[10] K. Tasaki, K. Kanda, S. Nakamura, M. Ue, J. Electrochem. Soc. 150 (2003) A1628.
[11] A.V. Plakhotnyk, L. Ernst, R. Schmutzler, J. Fluorine Chem. 126 (2005) 27.
[12] M.B. Armand, C.E.M.F. El Kadiri, United States Patent US 4505997 (1985).
[13] L.J. Krause, W. Lamanna, J. Summerfield, M. Engle, G. Korba, R. Loch, R. Atanasoski, J. Power Sources 68 (1997) 320.
[14] F. Kita, A. Kawakami, J. Nie, T. Sonoda, H. Kobayashi, J. Power Sources 68 (1997) 307.
[15] M. Xu, A. Xiao, W. Li, B.L. Lucht, J. Electrochem. Soc. 157 (2010) A115.

[16] N. Nanbu, K. Tsuchiya, T. Shibazaki, Y. Sasaki, Electrochem. Solid-State Lett. 5 (2002) A202.
[17] M. Eberwein, A. Schmid, M. Schmidt, M. Zabel, T. Burgemeister, J. Barthel, W. Kunz, H.J. Gores, J. Electrochem. Soc. 150 (2003) A994.
[18] M. Schmidt, U. Heider, A. Kuehner, R. Oesten, M. Jungnitz, N. Ignatev, P. Sartori, J. Power Sources 97–98 (2001) 557.
[19] J.S. Gnanaraj, M.D. Levi, Y. Gofer, D. Aurbach, M. Schmidt, J. Electrochem. Soc. 150 (2003) A445.
[20] F. Kita, H. Sakata, A. Kawakami, H. Kamizori, T. Sonoda, H. Nagashima, N.V. Pavlenko, Y.L. Yagupolskii, J. Power Sources 97–98 (2001) 581.
[21] L.A. Dominey, V.R. Koch, T.J. Blakley, Electrochim. Acta 37 (1992) 1551.
[22] J. Barthel, A. Schmid, H.J. Gores, J. Electrochem. Soc. 147 (2000) 21.
[23] Y. Sasaki, M. Handa, S. Sekiya, K. Kurashima, K. Usami, J. Power Sources 97–98 (2001) 561.
[24] H.S. Lee, X.Q. Yang, X. Sun, J. McBreen, J. Power Sources 97–98 (2001) 566.
[25] U. Wietelmann, U. Lischka, M. Wegner, United States Patent US 6506516 (2003).
[26] W. Xu, C.A. Angell, Electrochem. Solid-State Lett. 3 (2001) 366.
[27] K. Xu, S. Zhang, T.R. Jow, W. Xu, C.A. Angell, Electrochem. Solid-State Lett. 5 (2002) A26.
[28] K. Xu, S.S. Zhang, U. Lee, J.L. Allen, T.R. Jow, J. Power Sources 146 (2005) 79.
[29] H. Yamaguchi, H. Takahashi, M. Kato, J. Arai, J. Electrochem. Soc. 150 (2003) A312.
[30] T.J. Barbarich, P.F. Driscoll, Electrochem. Solid-State Lett. 6 (2003) A113.
[31] Z.-B. Zhou, M. Takeda, T. Fujii, M. Ue, J. Electrochem. Soc. 152 (2005) A351.
[32] S.S. Zhang, Electrochem. Commun. 8 (2006) 1423.
[33] J. Arai, A. Matsuo, T. Fujisaki, K. Ozawa, J. Power Sources 193 (2009) 851.
[34] M. Armand, P. Johansson, J. Power Sources 178 (2008) 821.
[35] J. Scheers, P. Johansson, P. Szczecinski, W. Wieczorek, M. Armand, P. Jacobsson, J. Power Sources 195 (2010) 6081.
[36] H. Matsumoto, H. Sakaebe, K. Tatsumi, M. Kikuta, E. Ishiko, M. Kono, J. Power Sources 160 (2006) 1308.
[37] M. Ishikawa, T. Sugimoto, M. Kikuta, E. Ishiko, M. Kono, J. Power Sources 162 (2006) 658.
[38] T. Sugimoto, M. Kikuta, E. Ishiko, M. Kono, M. Ishikawa, J. Power Sources 183 (2008) 436.
[39] A. Guerfi, S. Duchesne, Y. Kobayashi, A. Vijh, K. Zaghib, J. Power Sources 175 (2008) 866.
[40] S. Seki, Y. Kobayashi, H. Miyashiro, Y. Ohno, Y. Mita, N. Terada, P. Charest, A. Guerfi, K. Zaghib, J. Phys. Chem. C 11 (2008) 16708.
[41] K. Kubota, T. Nohira, T. Goto, R. Hagiwara, Electrochem. Commun. 10 (2008) 1886.
[42] G.B. Appetecchi, M. Montanino, A. Balducci, S.F. Lux, M. Winter, S. Passerini, J. Power Sources 192 (2009) 599.
[43] S.F. Lux, M. Schmuck, G.B. Appetecchi, S. Passerini, M. Winter, A. Balducci, J. Power Sources 192 (2009) 606.
[44] A.I. Bhatt, A.S. Best, J. Huang, A.F. Hollenkamp, J. Electrochem. Soc. 157 (2010) A66.
[45] Y. Wang, K. Zaghib, A. Guerfi, F.F.C. Bazito, R.M. Torresi, J.R. Dahn, Electrochim. Acta 52 (2007) 6346.
[46] E. Paillard, Q. Zhou, W.A. Henderson, G.B. Appetecchi, M. Montanino, S. Passerini, J. Electrochem. Soc. 156 (2009) A891.
[47] Q. Zhou, W.A. Henderson, G.B. Appetecchi, S. Passerini, J. Phys. Chem. C 114 (2010) 6201.
[48] A. Abouimrane, J. Ding, I.J. Davidson, J. Power Sources 189 (2009) 693.
[49] C. Michot, M. Armand, J.Y. Sanchez, Y. Choquette, M. Gauthier, United States Patent US 5916475 (1999).
[50] K. Zaghib, P. Charest, A. Guerfi, J. Shim, M. Perrier, K. Striebel, J. Power Sources 134 (2004) 124.
[51] K. Zaghib, P. Charest, A. Guerfi, J. Shim, M. Perrier, K. Striebel, J. Power Sources 146 (2005) 380.
[52] C. Michot, Canadian Patent CA 2527802 (2007).
[53] M. Beran, J. Prihoda, Z. Anorg. Allg. Chem. 631 (2005) 55.
[54] M. Beran, J. Prihoda, Z. Zak, M. Cernik, Polyhedron 25 (2006) 1292.
[55] M. Beran, J. Prihoda, J. Taraba, Polyhedron 29 (2010) 1292.
[56] H.-B. Han, Y.-X. Zhou, K. Liu, J. Nie, X.-J. Huang, M. Armand, Z.-B. Zhou, Chem. Lett. 39 (2010) 472.
[57] HyperChem™ Professional 7, Hypercube Inc., 1115 NW 4th Street, Gainesville, Florida 32601, USA.
[58] M. Ue, A. Murakami, S. Nakamura, J. Electrochem. Soc. 149 (2002) A1385.
[59] M. Ue, S. Mori, J. Electrochem. Soc. 142 (1995) 2577.
[60] G.Y. Gu, S. Bouvier, C. Wu, R. Laura, M. Rzeznik, K.M. Abraham, Electrochim. Acta 45 (2000) 3127.
[61] G.Y. Gu, R. Laura, K.M. Abraham, Electrochem. Solid-State Lett. 2 (1999) 486.
[62] M.S. Ding, J. Chem. Eng. Data 49 (2004) 1102.
[63] S.I. Smedley, The Interpretation of Ionic Conductivity in Liquids, Plenum, New York, 1980.
[64] G. Adam, J.H. Gibbs, J. Chem. Phys. 43 (1965) 139.
[65] M.H. Cohen, D. Turnbull, J. Chem. Phys. 31 (1959) 1164.
[66] P.E. Stallworth, J.J. Fontanella, M.C. Wintersgill, C.D. Scheidler, J.J. Immel, S.G. Greenbaum, A.S. Gozdz, J. Power Sources 81–82 (1999) 739.
[67] H. Yang, K. Kwon, T.M. Devine, J.W. Evans, J. Electrochem. Soc. 147 (2000) 4399.
[68] X. Wang, E. Yasukawa, S. Mori, Electrochim. Acta 45 (2000) 2677.
[69] W.K. Behl, E.J. Plichtar, J. Power Sources 72 (1998) 132.
[70] X. Zhang, T.M. Devine, J. Electrochem. Soc. 153 (2006) B375.